Impact of molecular structure as sticker–spacer model on formation and internal environments of coacervates composed of low-molecular-weight compounds

Sayuri L. Higashi[a,b,c]*, Ryutaro Fujimoto[d], Koichiro M. Hirosawa[e], Kenichi G.N. Suzuki[e,f,g], and Masato Ikeda[b,c,d,e,f]*

[a]Institute of Advanced Study, Gifu University, 1-1 Yanagido, Gifu 501-1193, Japan

[b]United Graduate School of Drug Discovery and Medical Information Sciences, Gifu University, 1-1 Yanagido, Gifu 501-1193, Japan

[c]Institute of Advanced Study, Center for One Medicine Innovative Translational Research (COMIT), Gifu University, 1-1 Yanagido, Gifu 501-1193, Japan

[d]Department of Life Science and Chemistry, Graduate School of Natural Science and Technology, Gifu University, 1-1 Yanagido, Gifu 501-1193, Japan

[e]Institute for Glyco-core Research (iGCORE), Gifu University, 1-1 Yanagido, Gifu 501-1193, Japan

[f]Innovation Research Center for Quantum Medicine, Graduate School of Medicine, Gifu University, 1-1 Yanagido, Gifu 501-1193, Japan

[g]Division of Advanced Bioimaging, National Cancer Center Research Institute (NCCRI), 5-1-1 Tsukiji, Chuo-ku, Tokyo 104-0045, Japan.

*Sayuri L. Higashi and Masato Ikeda

Email: higashi.sayuri.h0@f.gifu-u.ac.jp, ikeda.masato.n3@f.gifu-u.ac.jp

Keywords: coacervates, liquid–liquid phase separation, self-assembly, stimuli responsiveness, supramolecular materials

Abstract

Coacervates formed through liquid–liquid phase separation have been established as potential protocells. Unlike widely studied macromolecules, coacervates from low-molecular-weight compounds have recently gained importance because they provide simple but valuable *in vitro* models for biomolecular condensates and serve as promising platforms for the development of functional biomaterials. Herein, we present a modular molecular design for the phase separation of low-molecular-weight compounds containing two aromatic or cycloalkane stickers linked via a flexible hydrophilic spacer. These low-molecular-weight compounds self-assemble into micron-scale liquid-like coacervates at submillimolar concentrations. The coacervates provide a hydrophobic internal microenvironment that can selectively sequester hydrophobic guest molecules while excluding hydrophilic molecules. We demonstrate the controlled release of

https://doi.org/10.26434/chemrxiv-2025-8mns1 **ORCID:** https://orcid.org/0000-0001-8488-4808 Content not peer-reviewed by ChemRxiv. **License:** CC BY-NC-ND 4.0

hydrophobic drugs encapsulated in reduction-responsive coacervates composed of nitrophenyl groups as stickers that are cleaved by the addition of a reductant to induce the disassembly of the coacervates. This research is based on a rational molecular design for the construction of simple coacervates composed of low-molecular-weight compounds and offers an opportunity to construct more complicated coacervate-based protocell models and biofunctional soft materials.

Main Text

Introduction

Compartmentalization plays a crucial role in the spatiotemporal regulation of numerous biological functions in living systems. Many synthetic compartments have been designed using bottom-up approaches to create cell-like materials (1–4). Coacervates are formed spontaneously through the liquid–liquid phase separation (LLPS) of typical polyelectrolytes, such as nucleic acids and polypeptides, via multiple non-covalent interactions (5, 6). LLPS-induced coacervates have attracted considerable attention as mimics of protocell models relevant to the origin of life (7–10) and membraneless organelles (11, 12), which are also known as biomolecular condensates (13, 14). Although many studies have involved synthetic coacervates composed of various polyelectrolytes, their biocompatibility and applicability in living systems are limited by a lack of stability under biological conditions due to their high charge density and complex molecular structures (15). Recently, several research groups have synthesized phase-separating molecules based on low-molecular-weight compounds to create synthetic coacervates with multiple functions, including selective guest-molecule partitioning and acceleration of chemical (enzymatic) reactions (16). The simplification of molecular design could address the aforementioned challenges in coacervates and enable the implementation of new functions, such as responsiveness to specific stimuli, *e.g.,* pH (17–19), light (20–22), and redox reactions (17, 23), by incorporating stimuli-responsive molecular components, which is a well-developed strategy in the field of supramolecular hydrogels (24, 25). Recent studies have revealed that the sticker–spacer motif is an important structure in phase-separating (protein) molecules (17, 18, 21, 22, 26). Simple coacervates composed of fluorescent pyrene sticker–spacer-type molecules have been developed and applied for protein delivery into living cells (21). The authors synthesized and evaluated four additional sticker–spacer compounds (sticker: phenyl, naphthyl, trimethyl, or cyclopropyl groups); however, only one, which used dimeric naphthyl stickers, formed similar coacervates. Investigating coacervate-forming molecules will aid the development of new synthetic coacervates tailored for various applications. However, a deeper understanding of the physical properties, particularly the internal chemical environments, of guest partitioning depending on the molecular structures of the coacervate components remains scarce.

In this study, we designed and synthesized several sticker–spacer-type molecules with varying sticker parts and investigated their impact on the formation of coacervates (Fig. 1a). Moreover, we investigated their physical properties, including chemical stability, selective partitioning of guest molecules, and stimuli-responsive functions, to understand the influence of molecular-level changes in the sticker parts. Our findings provide important insights for the design of functional soft materials consisting of hierarchical structures, including coacervates, as key components of living cells.

Results and Discussion

Design and synthesis of phase-separating molecules and their coacervate formations

To develop phase-separating molecules, we designed and synthesized sticker–spacer-type low-molecular-weight compounds, namely, **OEG-bis-X** (**X** = **NPmoc**: 4-nitrophenylmethoxycarbonyl, **Pmoc**: phenylmethoxycarbonyl, and **cHex**: cyclohexylmethoxycarbonyl) (Scheme S1). Flexible and hydrophilic oligoethylene glycol (**OEG**) was used as the spacer, with X as the potential sticker

https://doi.org/10.26434/chemrxiv-2025-8mns1 **ORCID:** https://orcid.org/0000-0001-8488-4808 Content not peer-reviewed by ChemRxiv. **License:** CC BY-NC-ND 4.0

at both ends connected by carbamate bonds (Fig. 1a). The compounds were dissolved in dimethyl sulfoxide (DMSO) to prepare stock solutions (43 mM). When each **OEG-bis-X** DMSO stock solution was vigorously mixed with 100 mM phosphate buffer (pH 7.5) at ambient temperature, the solution immediately turned turbid (Fig. 1b), and spherical structures with diameters of up to several micrometers were clearly observed under an optical microscope (Fig. 1c). The micron-sized spherical structures, which can be defined as coacervates (*vide infra*), formed above a certain threshold concentration (~0.5 mM) (Fig. S17). The concentration of phosphate ions employed as buffering components affected the size of the coacervates, *i.e.*, smaller coacervates were formed at higher phosphate concentrations (Figs. 1d and S18). Importantly, the stochastically contacted coacervates spontaneously fused into larger coacervates within several tens of milliseconds, as shown in Fig. 1c (bottom), indicating liquid-like properties, and they exhibited Brownian motion, as expected for their sizes. In addition, wetting of the cover glass surface was frequently observed for the **OEG-bis-X** coacervates during microscopic observations (Fig. S19). We further examined the molecular dynamics of the coacervates using fluorescence recovery after photobleaching (FRAP) experiments with the coacervates stained with rhodamine 6G. After photobleaching a portion within the coacervates of **OEG-bis-NPmoc**, **OEG-bis-Pmoc**, **and OEG-bis-cHex**, rapid fluorescence recovery was observed, and the 50% fluorescence recovery times were estimated to be 5, 14, and 23 s, respectively (Fig. 1e). These results indicate that **OEG-bis-X** can self-assemble into simple liquid-like coacervates under aqueous conditions. In addition, the water contents of the **OEG-bis-NPmoc**, **OEG-bis-Pmoc**, and **OEG-bis-cHex** coacervates were 39 ± 4.1%, 68 ± 9.2%, and 52 ± 16%, respectively (Table 1 in Materials and Methods section), which is within the typical range reported for coacervates (from 40% to 90%) (13).

Next, we investigated the stability of the **OEG-bis-X** coacervates against NaCl, 1,6-hexanediol, and urea for comparison with simple biomolecular condensates composed of proteins (27–29). The addition of 5 M NaCl (final concentration of 1 M) barely affected the morphology of the three **OEG-bis-X** coacervates (Fig. S20). In contrast, 40% (*w*/*v*) 1,6-hexanediol (20% (*w*/*v*) final concentration) induced the dissolution of the **OEG-bis-Pmoc** and **OEG-bis-cHex** coacervates, which is consistent with liquid-like biomolecular condensates (30), but the mechanism is still unclear, while the **OEG-bis-NPmoc** coacervates were not significantly affected. This result suggests that the coacervate state of **OEG-bis-NPmoc** is stabilized by intermolecular interactions different not only from **OEG-bis-Pmoc** and **OEG-bis-cHex** but also from typical biomolecular condensates. In contrast, the addition of 15 M aqueous urea (final concentration of 5 M) had less effect on the morphology of all three **OEG-bis-X** coacervates (Fig. S20). This indicates that the destabilization of intermolecular hydrogen bonds induced by urea under these conditions is not effective for coacervate dissolution. Their stability against urea differs from that of simple biomolecular condensates (28, 29). Therefore, the **OEG-bis-X** coacervates showed resistance to changes in the chemical environment depending mainly on the chemical structure of the sticker group (**X**).

In addition, we surveyed the coacervate formation ability of **OEG-bis-X** bearing the stickers **nHex**: *n*-hexyloxycarbonyl, **2EtHex**: 2-ethyl-hexyloxycarbonyl, **nBut**: *n*-butyloxycarbonyl, **Alloc**: allyloxycarbonyl, and **moc**: methoxycarbonyl (Fig. S21a) to obtain further insights into the driving forces of coacervation. Because both **OEG-bis-Pmoc** (phenyl) and **OEG-bis-cHex** (cycloalkane) formed coacervates, π-π interactions may not be indispensable for coacervate formation, while their properties were different. **OEG-bis-nHex**, **OEG-bis-nBut** (linear alkanes), and **OEG-bis-2EtHex** (branched alkane) formed significantly smaller coacervates with an averaged diameter of 0.8 ± 0.5 μm (namely, mini-coacervates) compared to **OEG-bis-cHex** coacervates with an averaged diameter of 1.9 ± 0.8 μm (Fig. S21b). This indicates that the cycloalkane structure is more effective for the formation of coacervates. Nevertheless, **OEG-bis-nBut** formed similar coacervates at higher concentrations (43 mM), whose microscopic morphologies were comparable to that of **OEG-bis-cHex** coacervates (Figs. S21c and S22). In stark contrast, **OEG-bis-moc** did not form coacervates but gave only amorphous structures, which were rarely found at 4.3 mM and even at 43 mM (Fig. S22). Similarly, **OEG-bis-Alloc** showed no coacervate formation, even at 43 mM.

https://doi.org/10.26434/chemrxiv-2025-8mns1 **ORCID:** https://orcid.org/0000-0001-8488-4808 Content not peer-reviewed by ChemRxiv. **License:** CC BY-NC-ND 4.0

These indicate that the methyl and allyl groups were too short to induce effective coacervation for the molecular scaffold of **OEG-bis-X**.

Effects of sticker moieties in OEG-bis-X coacervates for selective partitioning of small molecule guests

To identify the physical properties of a coacervate, determining guest molecules partitioned into the dense phase, *i.e.*, the core, is essential. The selective exclusion from the coacervate or preferential uptake of guest molecules directly influences the downstream biochemical reactions that occur within this unique microenvironment (13). We investigated the ability of each **OEG-bis-X** coacervate to concentrate different fluorescent dyes (Nile red, fluorescein, tetramethylrhodamine ethyl ester (TMRE), and rhodamine B (RhoB)) using fluorescence microscopy (Figs. 2a–l). The encapsulation efficiency was calculated from the fluorescence intensity measurements of the dilute phase (Fig. 2s). All **OEG-bis-X** coacervates efficiently concentrated the hydrophobic Nile red with over 90% encapsulation efficiency (Figs. 2a–c and s). The lower fluorescence intensity of Nile red inside **OEG-bis-NPmoc** coacervates (Fig. 2a) compared with the **OEG-bis-Pmoc** or **OEG-bis-cHex** coacervates (Figs. 2b and c) might be due to **NPmoc** acting as a quencher for Nile red. In contrast, the uptake of hydrophilic fluorescein inside the coacervates appeared to be suppressed in all **OEG-bis-X** coacervates (Figs. 2d–f and s). These results suggest that the core of the **OEG-bis-X** coacervates were relatively hydrophobic compared to the dilute phase. The difference in the fluorescence intensity of zwitterionic TMRE and RhoB across all **OEG-bis-X** coacervates was consistent with their encapsulation efficiencies (Figs. 2g–l and s). These results indicated that slight differences in the chemical structures of the stickers influenced the uptake preferences of the coacervates. We further investigated selective guest partitioning using molecular rotors thioflavin T (ThT) and 9-(2,2-dicyanovinyl)julolidine (DCVJ) (31). For both ThT and DCVJ, the fluorescence intensity was the lowest inside the **OEG-bis-NPmoc** coacervates. Specifically, the fluorescence intensity of ThT was the highest inside **OEG-bis-Pmoc**, followed by **OEG-bis-cHex** with almost no significant differences in their encapsulation efficiencies (Figs. 2m–o and s). The fluorescence intensity of DCVJ was highest inside the **OEG-bis-cHex** coacervates, followed by **OEG-bis-Pmoc**, although no significant differences were found in the encapsulation efficiencies (Figs. 2p–r and s). These results imply that the bond rotation in ThT and DCVJ become restricted inside the hydrophobic coacervates most probably owing to the highly ordered molecular packing based on **Pmoc** or **cHex** moieties. In addition, the reversal between ThT (**Pmoc** > **cHex**) and DCVJ (**cHex** > **Pmoc**) suggests differences in internal microenvironment.

Reduction responsiveness of OEG-bis-NPmoc coacervates—Disassembly of OEG-bis-NPmoc coacervates by reduction stimuli

We evaluated the reduction responsiveness of an **NPmoc** group-containing molecule (**OEG-bis-NPmoc**) capable of constructing coacervates. As previously reported, chemical and enzymatic reductants can induce multi-electron reduction in **NPmoc** group (32), even under aqueous conditions, followed by releasing a quinoneimine methide fragment via irreversible *β*-1,6-elimination, as depicted in Fig. 3a. Hence, we prepared **OEG-bis-NPmoc** coacervates encapsulating doxorubicin hydrochloride (Fig. 3b) or Nile red (Fig. S23) as guest molecules. The coacervates disappeared within 20 min after adding an aqueous $Na_2S_2O_4$ (2.5 M, 7.5 μL, 30 eq. against **OEG-bis-NPmoc**) as a chemical reductant for the **NPmoc** group into aqueous mixtures containing **OEG-bis-NPmoc** coacervates (4.3 mM, 150 μL), even though small aggregates remained after 20 min (Fig. 3b and Movie S1). In contrast, the addition of tris(2-carboxyethyl)phosphine hydrochloride (TCEP; 1.0 eq. against **OEG-bis-NPmoc**) at a concentration sufficient to induce the cleavage of the assumed disulfide bond did not induce the disassembly of the **OEG-bis-NPmoc** coacervates (Figs. 3b and S23a). Furthermore, in the presence of $Na_2S_2O_4$, the turbidity of the solution containing **OEG-bis-NPmoc** coacervates decreased over time compared to that in the presence of TCEP (Figs. 3c and d). The reduction-responsive reaction of **OEG-bis-NPmoc** induced by $Na_2S_2O_4$ was analyzed by ^{1}H nuclear magnetic

https://doi.org/10.26434/chemrxiv-2025-8mns1 **ORCID:** https://orcid.org/0000-0001-8488-4808 Content not peer-reviewed by ChemRxiv. **License:** CC BY-NC-ND 4.0

resonance (NMR) spectroscopy (Figs. 3e and S24), whose samples were prepared after dissolution in a DMSO-d_6-D_2O (350 μL/300 μL) mixture (see the Supporting Information for details). The signals assignable to the nitrophenyl group ("a" and "b" protons, Fig. 3d) almost completely disappeared 30 min after adding $Na_2S_2O_4$, and multiple new peaks assignable to (hydroxyl)aminophenyl groups (6.8−7.6 ppm) appeared concurrently. In contrast, almost no spectral changes were observed upon the addition of TCEP. This selectivity was consistent with previous reports on **NPmoc**-containing molecules (33, 34). Collectively, these results indicate that the $Na_2S_2O_4$-induced, reduction-responsive disassembly of **OEG-bis-NPmoc** coacervate correlates with the chemical reduction of the nitro group and demonstrates a reduction-responsive release of encapsulated guest molecules from **OEG-bis-NPmoc** coacervates.

Conclusion

We successfully developed a series of simple sticker–spacer-type molecules, **OEG-bis-X** (**X** = **NPmoc**, **Pmoc**, **cHex**), capable of forming liquid-like coacervates through LLPS. By modifying the sticker motifs of **OEG-bis-X**, we identified the sticker motifs required for coacervate formation. In the previous report, the sticker-spacer type molecules composed of dimeric phenyl stickers connected by 3,6-dioxa-1,8-octanedithiol spacer did not form coacervates.(21) However, we newly found the sticker-spacer type molecules composed of dimeric benzyl stickers connected by a slightly longer oligoethylene glycol spacer are capable of forming coacervates. As reported by Abbas et al, not only hydrophobicity of stickers but also the chemical structures of the spacer, particularly its polarity, plays a crucial role in coacervate formation.(17) We evaluated the selective partitioning of various small molecule guests into these coacervates. All three types of coacervates exhibit hydrophobic microenvironments that sequester hydrophobic guest molecules while excluding hydrophilic guests. Notably, subtle differences in the sticker groups significantly influenced the uptake efficiency of zwitterionic dyes and the fluorescence intensity of molecular rotors inside these coacervates. This suggests that the sticker motifs not only affect guest partitioning but also modulate the internal properties of the coacervates, such as hydrophobicity or molecular packing density. We also demonstrated the reduction-responsive degradation of **OEG-bis-NPmoc** coacervates, which resulted in the release of the encapsulated guests. Further research on the dependence of sticker or spacer parts on stimuli responsiveness and guest-selective sequestration is in progress in our laboratory, as well as the detailed elucidation of the internal microenvironments of coacervates. Our findings contribute to the rational molecular design of coacervates for tailored applications in the fields of materials science and biotechnology.

Materials and Methods

General. Unless otherwise stated, all the commercial reagents were used as received. All water used in the experiments refers to ultra-pure water obtained from a Millipore system with a specific resistance of 18 MΩ•cm. Thin-layer chromatography was performed using a silica gel $60F_{254}$ (Merck). Column chromatography was performed on silica gel PSQ-100B (Fuji Silysia Chemical, 100 μm). ^1H and ^{13}C nuclear magnetic resonance (NMR) spectra were obtained using a JEOL JNM ECS-400 spectrometer (400 MHz for ^1H and 100 MHz for ^{13}C) with tetramethylsilane or residual non-deuterated solvents (1,4-dioxane or dimethyl sulfoxide (DMSO) for D_2O) as internal references. The multiplicities are abbreviated as follows: s = singlet, d = doublet, t = triplet, q = quartet, m = multiplet, dd = double doublet, and br = broad. Electrospray ionization mass spectrometry (ESI MS) was performed using a JEOL JMS-T100LP AccuTOF LC-plus mass spectrometer.

Preparation of coacervates. OEG-bis-X molecules were dissolved in DMSO (43 mM) as stock solution. Subsequently, 20 μL stock solution was added to 180 μL 100 mM sodium phosphate aqueous buffer (hereafter, phosphate buffer) (pH 7.5) in a vial container, following by immediate mixed using a vortex for 3 s to produce coacervates. The solution became milky-white. The coacervates were allowed to settle for approximately 5 min on a glass coverslip before imaging.

https://doi.org/10.26434/chemrxiv-2025-8mns1 **ORCID:** https://orcid.org/0000-0001-8488-4808 Content not peer-reviewed by ChemRxiv. **License:** CC BY-NC-ND 4.0

The coacervates were visualized using a fluorescence microscope (FV1000-D, IX81, Olympus, or BZ-X810, KEYENCE).

Turbidity measurements. All turbidity-based titrations were performed using an Infinite Pro200 TECAN M PLEX plate reader (Tecan Japan Co., Ltd., Osaka, Japan). Turbidity was used as an indicator of liquid–liquid phase separation for the samples in which the coacervates were observed by optical microscopy. Turbidity is defined as $\tau = -\ln(I/I_0)$, and can be calculated from the measured absorbance at a selected wavelength under the assumption that no light is absorbed at that particular wavelength. We used 600 nm for all turbidity measurements, and all measurements were performed in triplicate at room temperature. Turbidity was recorded after shaking the sample (200 µL) for 5 s. A well with the same volume (200 µL) of 100 mM phosphate buffer (pH 7.5)/DMSO (*v*/*v* = 9:1) was used as the blank.

Calculation of the water contents in OEG-bis-X coacervates. Following the procedure described in the literature (17), clean and empty glass vials were weighed (= m_e). **OEG-bis-X** coacervate samples (4.0 mL) were prepared in these vials, as described above. The vials were then centrifuged at 250× *g* for 1 h. After centrifugation, the supernatant was removed using a pipette and filter paper. The vials were again weighed (= m_c). Next, the vials were dried at 120 °C for 48 h. Finally, the dried vials were again weighed (= m_d). The water content, Q_w (%), was calculated as Q_w (%) = 100 × ($m_c - m_d$)/($m_c - m_e$).

Table 1. Water content of **OEG-bis-X** coacervates.

Derivatives (**X**)	Water content (%)
NPmoc	39 ± 4.1
Pmoc	68 ± 9.2
cHex	52 ± 16

Partitioning experiments and CLSM observation. OEG-bis-X (**X** = **NPmoc**, **Pmoc**, **cHex**) coacervates (4.3 mM, 100 mM phosphate buffer (pH 7.5)/DMSO (*v*/*v* = 9:1), 20 µL) obtained according to the procedure described above was spotted on a glass coverslip (diameter: 25 mm, thickness: 0.13–0.17 mm, Fisher Scientific) placed in an Attofluor cell chamber (Thermo Fisher Scientific), and then mixed with a DMSO solution of fluorescent dye (200 µM, 0.5 µL). Confocal laser scanning fluorescence microscopy (CLSM) observations were performed using an FV1000-D microscope (IX81, Olympus) equipped with a LD laser (559 nm) for Nile red, tetramethylrhodamine ethyl ester (TMRE), rhodamine B (RhoB), rhodamine 6G, and tetramethylrhodamine labeled dextrans (TMR-dextran), an Ar laser (488 nm) for fluorescein, Thioflavin T (ThT), and 9-(2,2-dicyanovinyl)julolidine (DCVJ), and a gallium arsenide phosphide (GaAsP) detector. A 60× (numerical aperture (NA) = 1.49) oil objective was employed to obtain images (typically 1024 × 1024 pixels). Images were obtained and analyzed using the acquisition software FV10-ASW4.2 equipped with a microscope.

FRAP analysis. Samples were prepared as described above using rhodamine 6G (final concentration of 0.5 µM). Fluorescence recovery after photobleaching (FRAP) measurements were performed using an FV1000-D microscope (IX81, Olympus) equipped with a Plan-Apochromat 100× (NA =1.49) oil objective and a GaAsP photo multiplier tube). Time-lapse movies were acquired with a scan area and rate of 128 × 128 pixels and 375 ms/frame, respectively. Photobleaching was conducted within a circular ROI in the middle of the coacervate of interest, bleaching with an LD laser (559 nm) at 100% laser power (3 s), and imaging for recovery was conducted continuously at reduced laser power (1%). To estimate the half recovery time ($\tau_{1/2}$), the photobleaching rate was calculated from the fluorescence of the background and unbleached

https://doi.org/10.26434/chemrxiv-2025-8mns1 **ORCID:** https://orcid.org/0000-0001-8488-4808 Content not peer-reviewed by ChemRxiv. **License:** CC BY-NC-ND 4.0

coacervate as a control, and the FRAP curve was corrected accordingly. The fluorescence intensity of the coacervates then curve-fitted using the exponential equation “One-phase association” in GraphPad Prism software. The data represent the mean ± standard deviation (SD).

Evaluation of the guest encapsulation efficiency (*E%*) of coacervates. After preparation of coacervate solution (200 μL) following the above procedure, a 200 μM dye solution (5.0 μL) was added to the mixture and mixed with a vortex for 3 s. The resulting mixture was left to equilibrate overnight at room temperature in the dark, followed by centrifugation at 6000× *g* at 25 °C for 1 min. As a control, the 200 μM dye solution (5.0 μL) was added to the mixture of DMSO without **OEG-bis-X** (20 μL) and 100 mM phosphate buffer (pH 7.5, 180 μL). Fifty microliters of the supernatant or control were diluted with 150 μL of the appropriate solvent (DMSO: Nile red and TMRE; ethanol: RhoB; Milli-Q: fluorescein; 75% glycerol: DCVJ and ThT) followed by measurement of the fluorescence intensity using the plate reader. The supernatant concentration (c_s) was obtained from a standard curve prepared from a series of samples with known concentrations (35, 36). The encapsulation efficiency *E%* was calculated as follows: $E\% = 100 \times (c_t - c_s)/c_t$, where c_t is the set total concentration.

Reduction-induced coacervate disassembly. Typically, to a solution containing **OEG-bis-NPmoc** coacervates (4.3 mM, 100 mM phosphate buffer (pH 7.5)/DMSO (*v*/*v* = 9:1, 150 μL)) was added an aqueous solution of $Na_2S_2O_4$ (2.5 M, 7.5 μL, 30 eq.) The resulting sample was incubated at room temperature for the designated time. Stimuli-responsive disassembly was carefully evaluated using fluorescence and optical microscopy, turbidity measurements, and ^{1}H NMR spectroscopy according to a previous report (34). As negative control experiments, an aqueous solution of TCEP (10 mM, 8.6 μL, 1 eq.) was added instead of an aqueous solution of $Na_2S_2O_4$.

Supporting information
Supporting Information, including Figures S1–S24, synthesis and characterization of **OEG-bis-X**.

Acknowledgments

This work was supported in part by JSPS KAKENHI (23K19212 and 24H01126 to S.L.H., and 23H01815 to M. I.), Tokai Pathways to Global Excellence (T-GEx), the MEXT Strategic Professional Development Program for Young Researchers (S.L.H.), and Toyota Riken Research Grants. The authors thank Editage (www.editage.jp) for English language review.

References

1. B. C. Buddingh’, J. C. M. van Hest, Artificial cells: Synthetic compartments with life-like functionality and adaptivity. *Acc. Chem. Res.* **50**, 769–777 (2017).
2. I. Insua, J. Montenegro, Synthetic supramolecular systems in life-like materials and protocell models. *Chem.* **6**,1652–1682 (2020).
3. L. Tanwar, N. K. Devaraj, Engineering materials for artificial cells. *Curr. Opin. Solid State Mater. Sci.* **26**, 101004 (2022).
4. C. Guindani, L. C. Da Silva, S. Cao, T. Ivanov, K. Landfester, Synthetic cells: From simple bio-inspired modules to sophisticated integrated systems. *Angew. Chem. Int. Ed.* **61**, e202110855 (2022).
5. F. W. Tiebackx, Gleichzeitige Ausflockung zweier Kolloide. *Z. Chem. Ind. Koll.* **8**, 198–201 (1911).
6. B. de Jong, H. R. Kruyt, Coacervation. *Proc. R. Acad. Amsterdam* **32**, 849–856 (1929).
7. A. I. Oparin, Evolution of the concepts of the origin of life. *Origins Life* **7**, 3−8 (1976).
8. B. Ghosh, R. Bose, T-Y. Dora Tang, Can coacervation unify disparate hypotheses in the origin of cellular life? *Curr. Opin. Colloid Interface Sci.* **52**, 101415 (2021).

https://doi.org/10.26434/chemrxiv-2025-8mns1 **ORCID:** https://orcid.org/0000-0001-8488-4808 Content not peer-reviewed by ChemRxiv. **License:** CC BY-NC-ND 4.0

9. Z. Lin, T. Beneyton, J.-C. Baret, N. Martin, Coacervate droplets for synthetic cells. *Small Methods,* **7**, 2300496 (2023).
10. S. Kuila, J. Nanda, Cysteine-based dynamic self-assembly and their importance in the origins of life. *ChemSystemsChem*, **6**, e202400022 (2024).
11. C. P. Brangwynne, C. R. Eckmann, D. S. Courson, A. Rybarska, C. Hoege, J. Gharakhani, F. Jülicher, A. A. Hyman, Germline P granules are liquid droplets that localize by controlled dissolution/condensation. *Science* **324**, 1729–1732 (2009).
12. Y. Shin, C. P. Brangwynne, Liquid phase condensation in cell physiology and disease. *Science* **357**, eaaf4382 (2017).
13. N. A. Yewdall, A. A. André, T. Lu, E. Spruijt, Coacervates as models of membraneless organelles. *Curr. Opin. Colloid Interface Sci.* **52**, 101416 (2021).
14. A. B. Cook, S. Novosedlik, J. C. M. Van Hest, Complex coacervate materials as artificial cells. *Acc. Mater. Res.* **4**, 287–298 (2023).
15. M. H. M. E. van Stevendaal, L. Vasiukas, N. A. Yewdall, A. F. Mason, J. C. M. van Hest, Engineering of biocompatible coacervate-based synthetic cells. *ACS Appl. Mater. Interfaces* **13**, 7879–7889 (2021).
16. S. L. Higashi, M. Ikeda, Coacervates composed of low-molecular-weight compounds–molecular design, stimuli responsiveness, confined reaction. *Adv. Biol.*, https://doi.org/10.1002/adbi.202400572 (2025).
17. M. Abbas, W. P. Lipiński, K. K. Nakashima, W. T. S. Huck, E. Spruijt, A short peptide synthon for liquid–liquid phase separation**.** *Nat. Chem.* **13**, 1046–1054 (2021).
18. M. Abbas, J. O. Law, S. N. Grellscheid, W. T. S. Huck, E. Spruijt, Peptide-based coacervate-core vesicles with semipermeable membranes. *Adv. Mater.* **34**, 2202913 (2022).
19. S. Cao, T. Ivanov, J. Heuer, C. T. J. Ferguson, K. Landfester, L. C. da Silva, Dipeptide coacervates as artificial membraneless organelles for bioorthogonal catalysis. *Nat. Commun.* **15**, 39 (2024).
20. R. Kubota, S. Torigoe, I. Hamachi, Temporal stimulus patterns drive differentiation of a synthetic dipeptide-based coacervate. *J. Am. Chem. Soc.* **144**, 15155–15164 (2022).
21. Y. Bao, H. Chen, Z. Xu, J. Gao, L. Jiang, J. Xia, Photo-responsive phase-separating fluorescent molecules for intracellular protein delivery. *Angew. Chem. Int. Ed.* **62**, e202307045 (2023).
22. J. Xia, H. Kong, X. Xie, Y. Bao, F. Zhang, L. Bian, K. Cheng, Y. Zhao, Phase-Separated Spiropyran Coacervates as Dual-Wavelength-Switchable Reactive Oxygen Generators. *Angew. Chem. Int. Ed.*, e202419538 (2025).
23. Y. Yan, W. Mu, H. Li, C. Song, Y. Qiao, Y. Lin, Dynamical behaviors of oscillating metallosurfactant coacervate microdroplets under redox stress. *Adv. Mater.* **35**, 2210700 (2023).
24. H. Shigemitsu, I. Hamachi, Design strategies of stimuli-responsive supramolecular hydrogels relying on structural analyses and cell-mimicking approaches. *Acc. Chem. Res.* **50**, 740–750 (2017).
25. H. Zhou, Y. Zhu, B. Yang, Y. Huo, Y. Yin, X. Jiang, W. Ji, Stimuli-responsive peptide hydrogels for biomedical applications. *Mater. Chem. B* **12**, 1748–1774 (2024).
26. E. W. Martin, A. S. Holehouse, I. Peran, M. Farag, J. J. Incicco, A. Bremer, C. R. Grace, A. Soranno, R. V. Pappu, T. Mittag, Valence and patterning of aromatic residues determine the phase behavior of prion-like domains. *Science* **367**, 694–699 (2020).
27. G. Krainer, T. J. Welsh, J.A. Joseph, J. R. Espinosa, S. Wittmann, E. de Csilléry, A. Sridhar, Z. Toprakcioglu, G. Gudiškytė, M. A. Czekalska, W. E. Arter, J. Guillén-Boixet, T. M. Franzmann, S. Qamar, P. St George-Hyslop, A. A. Hyman, R. Collepardo-Guevara, S. Alberti, T. P. J. Knowles, Reentrant liquid condensate phase of proteins is stabilized by hydrophobic and non-ionic interactions. *Nat. Commun.* **12**, 1085 (2021).
28. M. Poudyal, K. Patel, L. Gadhe, A. S. Sawner, P. Kadu, D. Datta, S. Mukherjee, S. Ray, A. Navalkar, S. Maiti, D. Chatterjee, J. Devi, R. Bera, N. Gahlot, J. Joseph, R. Padinhateeri, S. K. Maji, Intermolecular interactions underlie protein/peptide phase separation irrespective of sequence and structure at crowded milieu. *Nat. Commun.* **14**, 6199 (2023).

https://doi.org/10.26434/chemrxiv-2025-8mns1 **ORCID:** https://orcid.org/0000-0001-8488-4808 Content not peer-reviewed by ChemRxiv. **License:** CC BY-NC-ND 4.0

29. S. Rai, S. Pramanik, S. Mukherjee, Deciphering the liquid–liquid phase separation induced modulation in the structure, dynamics, and enzymatic activity of an ordered protein β-lactoglobulin. *Chem. Sci.* **15**, 3936–3948 (2024).
30. S. Kroschwald, S. Maharana, A. Simon, Hexanediol: A chemical probe to investigate the material properties of membrane-less compartments. *Matters* **3**, 201702000010 (2017).
31. S. Nagarajan, L. J. Lapidus, Fluorescent Probe DCVJ Shows High Sensitivity for characterization of amyloid b-peptide early in the lag phase. *ChemBioChem* **18**, 2205–2211 (2017).
32. S. L. Higashi, Y. Shintani, M. Ikeda, Installing reduction responsiveness into biomolecules by introducing nitroaryl groups. *Chem. Eur. J.* **28**, e202201103 (2022).
33. M. Ikeda, T. Tanida, T. Yoshii, K. Kurotani, S. Onogi, K. Urayama, I. Hamachi, Installing logic-gate response to a variety of biological substances in supramolecular hydrogel-enzyme hybrids. *Nat. Chem.* **6**, 511–518 (2014).
34. S. L. Higashi, M. Ikeda, Development of an amino sugar-based supramolecular hydrogelator with reduction responsiveness. *JACS Au* **1**, 1639–1646 (2021).
35. B. K. C, T. Nii, T. Mori, Y. Katayama, A. Kishimura, Dynamic frustrated charge hotspots created by charge density modulation sequester globular proteins into complex coacervates. *Chemi. Sci.* **14**, 6608–6620 (2023).
36. P. Chowdhury, B. Saha, K. Bauri, B. S. Sumerlin, P. De, Hydrogen bonding-driven self-coacervation of nonionic homopolymers for stimuli-triggered therapeutic release. *J. Am. Chem. Soc.* **146**, 21664–21676 (2024).

https://doi.org/10.26434/chemrxiv-2025-8mns1 **ORCID:** https://orcid.org/0000-0001-8488-4808 Content not peer-reviewed by ChemRxiv. **License:** CC BY-NC-ND 4.0

Figures

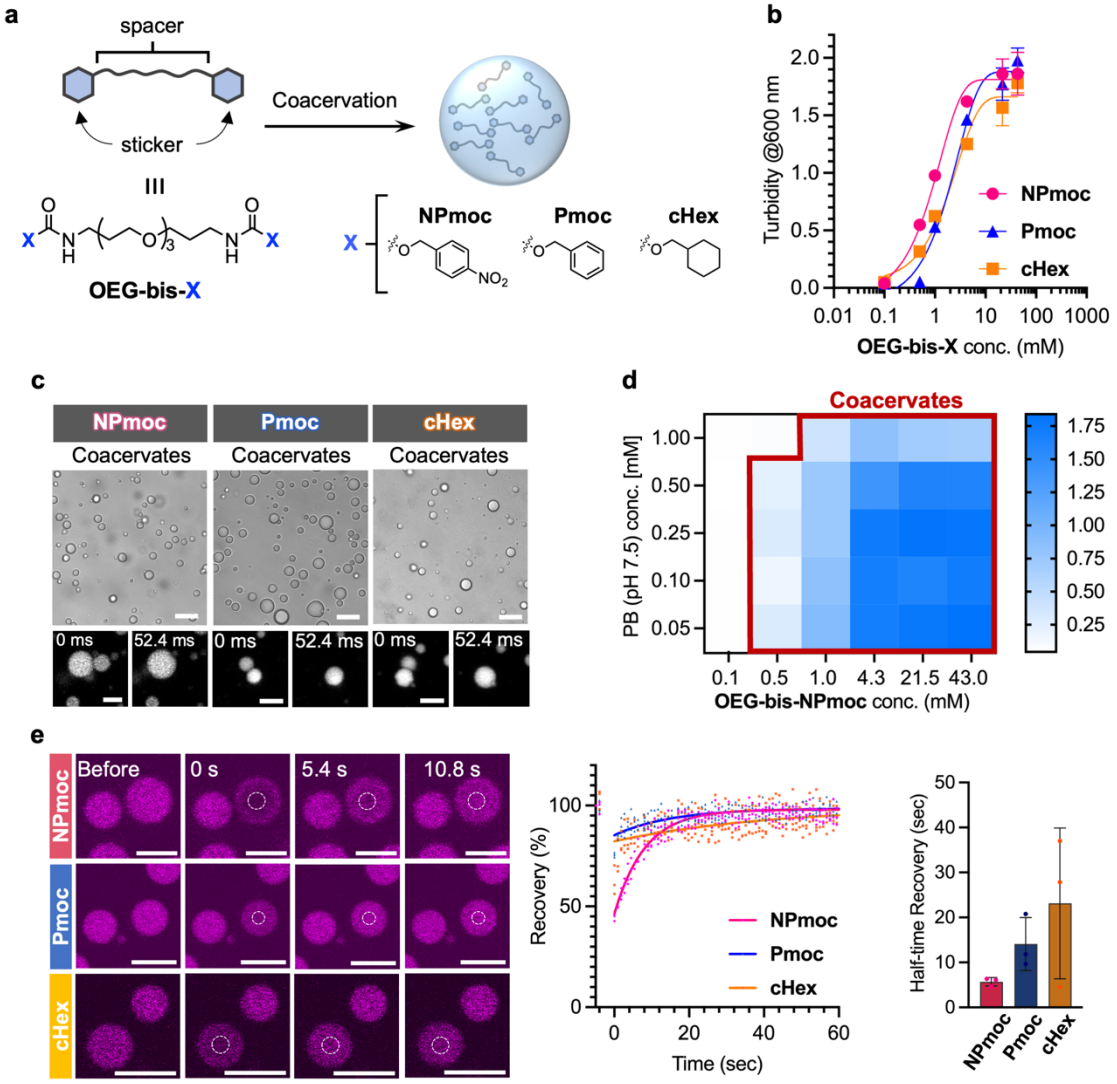

Figure 1. (**a**) Chemical structures of **OEG-bis-X** (**X** = **NPmoc**, **Pmoc**, **cHex**) and schematic of coacervation. (**b**) Turbidity (OD_{600}) of solutions containing **OEG-bis-X** at different concentrations in 100 mM phosphate buffer (pH 7.5)/DMSO (*v*/*v* = 9:1). The lines between points are eye guides. Error bars indicate the standard deviation (SD) of the average OD_{600} ($n = 3$). (**c**) Representative CLSM images (top: DIC, bottom: fluorescence, time lapse) of the **OEG-bis-X** coacervates. [**OEG-bis-X**] = 4.3 mM and [Nile red] = 5.0 μM in 100 mM phosphate buffer (pH 7.5)/DMSO (*v*/*v* = 9:1) at ambient temperature. Scale bar: 10 μm (top) and 5 μm (bottom). (**d**) Turbidity (OD_{600}) map for aqueous mixtures of **OEG-bis-NPmoc** (phosphate buffer (pH 7.5)/DMSO (*v*/*v* = 9:1)) at different **OEG-bis-NPmoc** and phosphate concentrations. (**e**) FRAP analysis showing the recovery of the Rhodamine 6G fluorescence within the coacervates after photobleaching. [**OEG-bis-X**] = 4.2 mM and [Rhodamine 6G] = 0.5 μM in 100 mM phosphate buffer (pH 7.5)/DMSO (*v*/*v* = 9:1) at ambient temperature. Scale bar: 5 μm. Data are presented as the mean ± SD ($n = 3$).

https://doi.org/10.26434/chemrxiv-2025-8mns1 **ORCID:** https://orcid.org/0000-0001-8488-4808 Content not peer-reviewed by ChemRxiv. **License:** CC BY-NC-ND 4.0

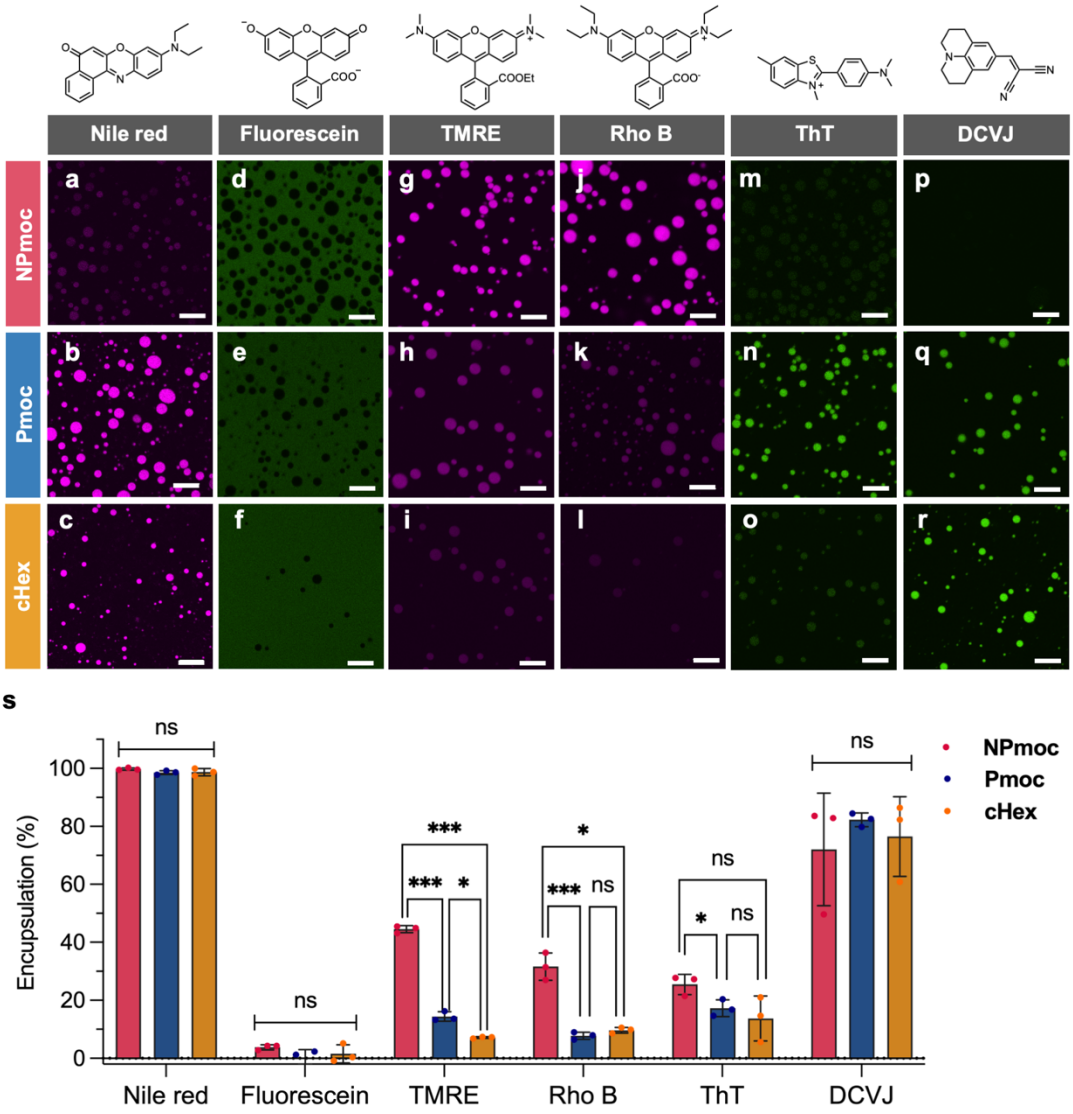

Figure 2. Partitioning of guest molecules in **OEG-bis-X** coacervates. Representative CLSM images of **OEG-bis-X** coacervates incubated with (**a**–**c**) Nile red, (**d**–**f**) fluorescein, (**g**–**i**) TMRE, (**j**–**l**) RhoB, (**m**–**o**) DCVJ, and (**p**–**r**) ThT. (**s**) The guest encapsulation efficiency (%) of the coacervates. [**OEG-bis-X**] = 4.2 mM and [dye] = 5.0 μm in 100 mM phosphate buffer (pH 7.5)/DMSO (*v*/*v* = 9:1) at ambient temperature. Scale bar: 10 μm.

https://doi.org/10.26434/chemrxiv-2025-8mns1 **ORCID:** https://orcid.org/0000-0001-8488-4808 Content not peer-reviewed by ChemRxiv. **License:** CC BY-NC-ND 4.0

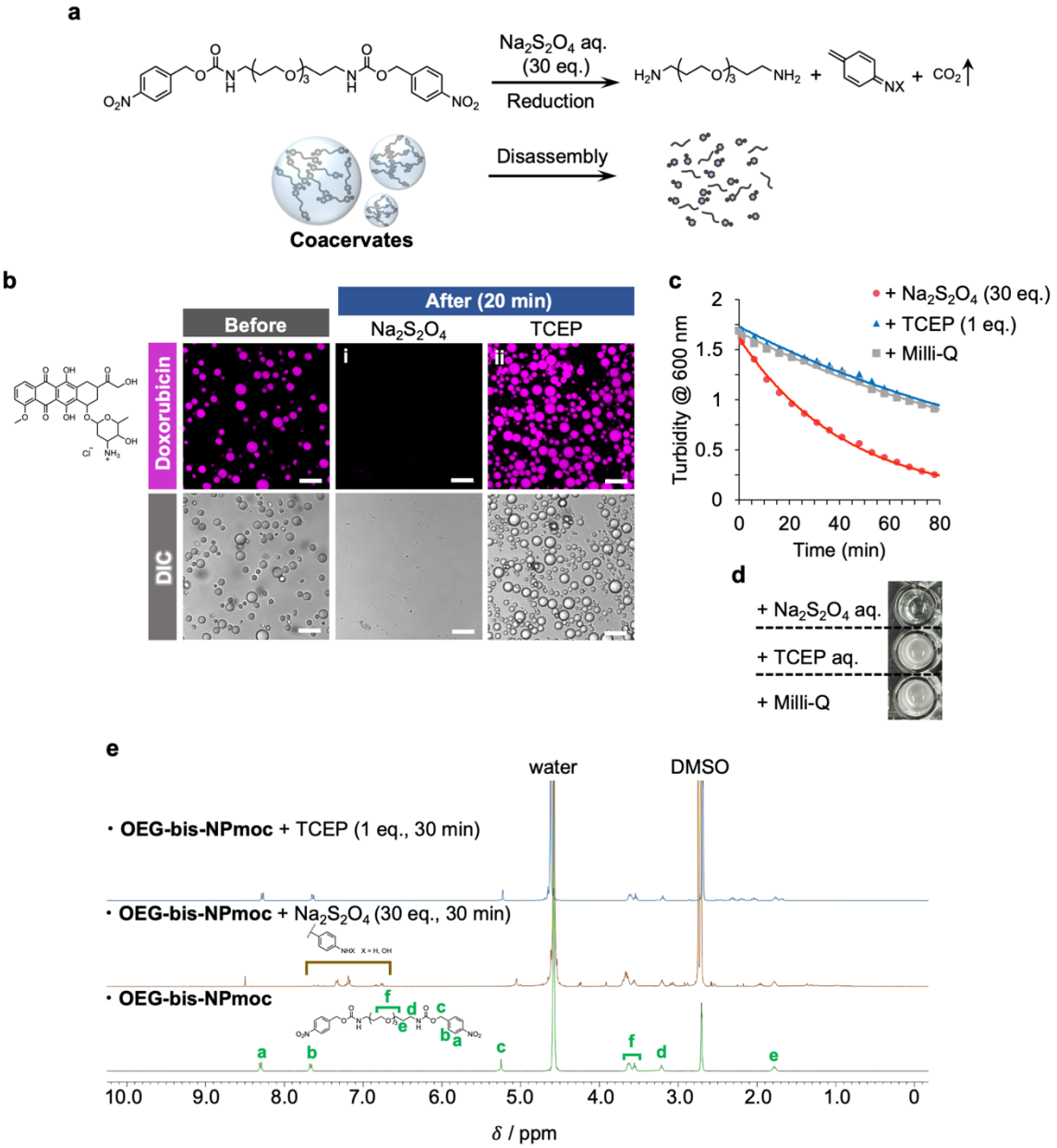

Figure 3. Reduction-stimulus responsiveness of **OEG-bis-NPmoc** coacervates. (**a**) Plausible scheme of the reduction reaction of **OEG-bis-NPmoc** induced by $Na_2S_2O_4$ and schematic of the reduction-responsive disassembly of **OEG-bis-NPmoc** coacervates. (**b**) Representative CLSM images of the **OEG-bis-NPmoc** coacervates before and after the addition of (**i**) $Na_2S_2O_4$ (20 min) and (**ii**) TCEP (20 min) at ambient temperature. [**OEG-bis-NPmoc**] = 4.2 mM and [Doxorubicin] = 20 μM in 100 mM phosphate buffer (pH 7.5)/DMSO (*v*/*v* = 9:1). (**i**) 2.5 M $Na_2S_2O_4$ aqueous solution (7.5 μL, 30 eq. against **OEG-bis-NPmoc**) or (**ii**) 84 mM TCEP aqueous solution (7.5 μL, 1.0 eq. against **OEG-bis-NPmoc**) was added to the coacervates solution (150 μL). Scale bar: 10 μm. (**c**) Turbidity (OD_{600}) of solutions containing **OEG-bis-NPmoc** coacervates before and after the addition of 2.5 M $Na_2S_2O_4$ (10 μL, 30 eq. against **OEG-bis-NPmoc**, red plots), 84 mM TCEP (10 μL, 1 eq. against **OEG-bis-NPmoc**, blue plots), or Milli-Q (10 μL, gray plots: overlapped with blue plots). The lines between points are eye guides. [**OEG-bis-NPmoc**] = 4.3 mM in 100 mM phosphate buffer (pH 7.5)/DMSO (*v*/*v* = 9:1). Error bars indicate the SD of the average OD_{600} (n = 3). (**d**)

https://doi.org/10.26434/chemrxiv-2025-8mns1 **ORCID:** https://orcid.org/0000-0001-8488-4808 Content not peer-reviewed by ChemRxiv. **License:** CC BY-NC-ND 4.0

Photographs of solutions containing **OEG-bis-NPmoc** coacervates 80 min after the addition of each solution in a microplate. (**e**) ^{1}H NMR spectra (400 MHz, DMSO-d_6/D_2O (*v*/*v* = 7/6), room temperature) (bottom) before and (top) after the addition of TCEP (1 eq.) or (middle) $Na_2S_2O_4$ (30 eq.) to **OEG-bis-NPmoc** coacervates (4.3 mM).

https://doi.org/10.26434/chemrxiv-2025-8mns1 **ORCID:** https://orcid.org/0000-0001-8488-4808 Content not peer-reviewed by ChemRxiv. **License:** CC BY-NC-ND 4.0